Front. Phys. China, 2010, 5(4): 405–413
DOI 10.1007/s11467-010-0131-6

MINI-REVIEW ARTICLE

In situ characterization of optoelectronic nanostructures and nanodevices

Min GAO (高旻)†, **Cheng-yao LI** (李成垚), **Wen-liang LI** (李文亮), **Xiao-xian ZHANG** (张小娴), **Lian-mao PENG** (彭练矛)

Key Laboratory for the Physics and Chemistry of Nanodevices, and Department of Electronics, Peking University, Beijing 100871, China
E-mail: †mingao@pku.edu.cn

Received May 20, 2010; accepted June 7, 2010

One-dimensional (1-D) semiconductor nanostructures can effectively transport electrons and photons, and are considered to be promising building blocks for future optoelectronic nanodevices. In this review, we present our recent efforts to integrate optical techniques and *in situ* electron microscopy for comprehensively characterizing individual 1-D optoelectronic nanostructures and nanodevices. The technical strategies and their applications in "green" emission and optical confinement in 1-D ZnO nanostructures will be introduced. We also show *in situ* assembly and characterization of nanostructures for optoelectronic device purposes. Using these examples, we demonstrate that the combination of optical techniques and *in situ* electron microscopy can be powerful for the studies of optoelectronic nanomaterials and nanodevices.

Keywords one-dimensional (1-D) semiconductor nanostructure, optoelectronic nanodevices, *in situ* electron microscopy, optical confinement, deep level emission

PACS numbers 78.67.-n, 78.55.-m, 78.60.Hk, 68.37.Hk

Contents

1 Introduction 405
2 Strategies to integrate optical characterization and *in situ* electron microscopy 406
2.1 Combination of micro-PL and *in situ* electron microscopy 406
2.2 Integrated system based on a SEM 406
3 Characterization of surface defects and deep level emission in ZnO nanowires 407
4 Characterization of optical confinement in 1-D ZnO nanostructures 409
5 *In situ* assembly and characterization of optoelectronic nanostructures for device purposes 411
6 Summary 412
Acknowledgements 412
References 412

1 Introduction

Nanomaterials exhibit unique physical properties mainly due to the large surface/volume ratio and the confinement effects. Among the various nanomaterials, one-dimensional (1-D) semiconductor nanostructures are considered to be promising building blocks for future electronic and optoelectronic nanodevices owning to their abilities to effectively transport electrons and photons [1–4]. A variety of miniaturized optoelectronic devices, e.g., light emitting diodes, nanolasers, detectors, and optical waveguides have been fabricated successfully based on individual 1-D nanostructures [5–17]. The above recent developments in nano-optoelectronics require not only nanoscale manipulation and processing of semiconducting nanostructures, but also characterization of optical, electrical and structural properties with resolution and sensitivity of individual nanostructures. In addition, the electrical and optical properties of optoelectronic nanodevices are closely correlated and are often required to be measured simultaneously. If we further consider the considerable inhomogeneity of as-grown nanomaterials, co-measurements of different aspects of the nanostructures, e.g., microstructure, composition, and electrical and optical properties, based on the same individual nanostructures are often essential for

a direct "structure-properties" correlation [18, 19].

The recent instrumentation developments of electron microscopy, a major tool of microstructural and compositional characterization of nanomaterials, have incorporated nanomanipulation and electrical measurement [20–25]. This trend is represented by the scanning probe stage inside transmission electron microscope (TEM) [20, 21] and the nanoprobe technique inside scanning electron microscope (SEM) [22–25]. For example, by controlling nanometer-sized metal tips with nanomanipulators, electrical contacts can be made to individual nanostructures inside SEM, thus *in situ* electrical measurements can be carried out [22–24]. For optical characterization of individual nanostructures, microphotoluminescence (micro-PL), [26–28] scanning near field optical microscopy [28–30] and cathodoluminescence (CL) inside SEM [30–32] are often employed. The integration of CL and SEM or a scanning transmission electron microscope can be traced back to several decades ago [33, 34]. Compared to the optical apparatuses attached TEM or STEM [33, 35], the SEM based CL spectroscopy and imaging have been used more widely in characterizing semiconductors due to the advantages of larger space, easier integration of cold stage and relatively lower damages. A typical modern SEM-based CL attachment includes a paraboloidal mirror just above the sample. The electron beam goes through a small hole on top of the mirror and excites the sample, while the generated luminescence is collected by the mirror and directed to the analyzer [36, 37]. A drawback of this type of optical attachment is that the sizeable mirror may block most other detectors and the nanoprobe attachment, thus hindering the co-measurement of electrical and optical properties of nanodevices and nanomaterials.

Partly driven by the challenges raised by the 1-D optoelectronic nanostructures, we have adopted two strategies to combine optical techniques and *in situ* scanning electron microscopy to achieve comprehensive characterization of the same individual nanostructure. In this review, we summarize our recent technical developments and their applications in studying the deep level emission and the waveguiding behavior in 1-D ZnO nanostructures, and *in situ* assembly and characterization of optoelectronic nanostructures for device purposes. Using these examples, we demonstrate that the combination of optical techniques and electron microscopy can be useful for nanomaterial and nanodevice studies.

2 Strategies to integrate optical characterization and *in situ* electron microscopy

Two straightforward technical approaches have been adapted: (1) *in situ* electron microscopy and microphotoluminescence are used separately to locate and measure the same individual nanostructure in a compatible sample [18]; (2) a comprehensive characterization system is assembled by combining space-saving fiber optics and *in situ* nanomanipulation technique inside a scanning electron microscope [19].

2.1 Combination of micro-PL and *in situ* electron microscopy

Figure 1 illustrates the comprehensive characterization on an individual suspended ZnO nanowire [Fig. 1(a)] by the combination of *in situ* SEM and micro-PL. We prepared the suspended nanowire samples by attaching an individual nanowire to nanometer-sized tungsten (W) tip using *in situ* SEM nanomanipulation and localized carbon deposition, which has been described in Refs. [19, 21]. Such "nanostructure-on-a-tip" configuration can also be used for micro-PL measurement. Using a chain of ZnO nanowires with special features, we show in Fig. 1(b) that the same nanowire can be located in the same orientation using SEM and a micro-PL optical system. Employment of such suspended individual nanowires provides a technique compatible with established electrical measurement using the *in situ* nanoprobe technique inside SEM [24]. Figure 1(c) is a typical *in situ* I–V curve of the individual ZnO nanowires with the W tip and Pt wire as electrodes. Figure 1(d) shows a typical PL spectrum of suspended individual ZnO nanowires. Similar to some of the previous reports [38], the PL spectra of the as-grown nanowires consist of a UV near band edge (NBE) emission peak and a broad defect-related deep level emission at ∼520 nm. Thus, microstructural (SEM), electrical (nanoprobe technique) and optical (PL) characterization can be carried out on the same nanowire.

2.2 Integrated system based on a SEM

Figure 2(a) shows a schematic configuration of the comprehensive characterization system assembled based on SEM. To incorporate optical characterization in the SEM, one or two optical fiber probes are attached to nano-manipulators, while the rest of the four manipulators still operate nanometer-sized W tips. Figure 2(b) is a digital photograph showing an optical fiber probe and two sharp metal tips operated by nanomanipulators. The outside end of the fiber probe is coupled to either a spectrometer for light analysis or a laser for optical excitation. The inside end of the fiber probe is either flat to enhance the angular resolving power or with a tip micro-lens to increase the light collection efficiency. The nano-manipulators enable 3-dimensional and nanometer accuracy movement of the fiber probes. Thus, the fiber probe can be routinely placed several microns away from

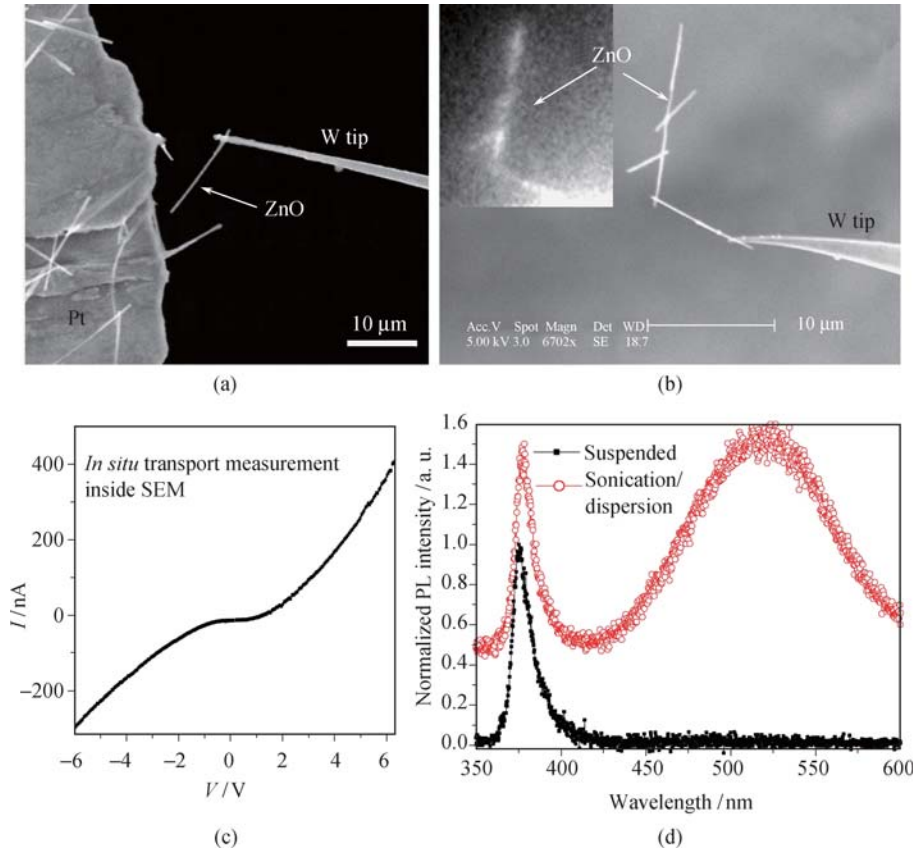

Fig. 1 **(a)** SEM image illustrating the preparation of suspended individual nanowires by nanoprobe manipulation inside SEM. **(b)** SEM and optical (*the inset*) images showing the same chain of ZnO nanowires glued to a W tip. **(c)** A typical $I-V$ curve obtained from individual suspended ZnO nanowires by *in situ* 2-terminal transport measurement using nanoprobe technique inside SEM. **(d)** Micro-PL spectra of an individual suspended as-grown ZnO nanowire and an individual ZnO nanowire processed by sonication/dispersion procedure. The two nanowires have regular cross-section and similar diameters (∼50 nm). Reprinted with permission from Ref. [18].

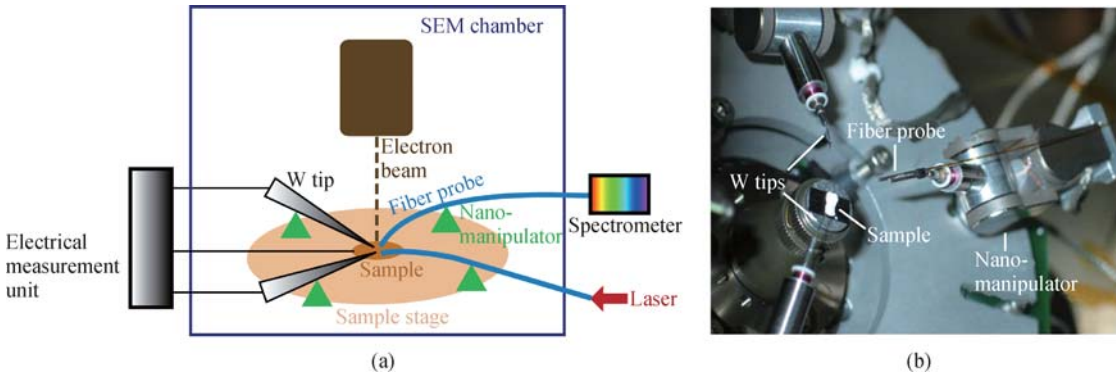

Fig. 2 **(a)** Schematic configuration of the integrated SEM system equipped with optical fibers and sharp metal probes controlled by nano-manipulators. **(b)** A digital photograph of part of the integrated SEM system. Reprinted with permission from Ref. [19].

the interesting areas for high efficiency optical detection or excitation. In contrast to the paraboloidal mirror light collector which blocks most other detectors, the space-saving design of the fiber probe component permits simultaneous action of the fiber probe and other SEM attachments (e.g., nanoprobe and EDS). By combining the above fiber optical attachment and the well-established *in situ* SEM techniques, a variety of characterization functions can be performed on the same individual nanostructures.

3 Characterization of surface defects and deep level emission in ZnO nanowires

Because of the much increased surface/volume ratio compared to the bulk materials, the surface defects often play an important role in the physical properties of 1-D nanos-

tructures. For example, the so-called "green" emission in ZnO nanostructures has been commonly considered to be related to surface defect and have complicated influences on the optical and electrical properties of the ZnO nanostructures [38–42]. Such defect-related deep level emission has been widely investigated; however, its origin is still under debate [38–42]. Using *in situ* burnt-out ZnO nanowires, we show that the comprehensive characterization yields insights on the green emission of ZnO nanowires.

A ∼3 μA current was applied to a ∼20-μm-long nanowire suspended between two tungsten (W) tips. The accumulated heating eventually resulted in a "burnt-out" near the center of the nanowires. Figure 3(a) and (b) shows SEM images of the nanowires before and after the burnt-out. The variations of O/Zn ratio and electrical conductance were monitored by energy dispersive X-ray spectroscopy (EDS) and electrical transport measurements using the W tips as electrodes [Fig. 3(c) and (d)]. The EDS spectra [Fig. 3(c)] taken from the same position before and after heating, indicates a remarkable oxygen loss (>5% in the areas close to the "burnt-out" point) during the *in situ* annealing process. On the other hand, the electrical conductance [Fig. 2(d)] first increases and then decreases even before the observable change in the nanowire shape. This is probably corresponding to the increase of carrier density and decrease of carrier mobility during the *in situ* annealing process in vacuum. The upper part of the "burnt-out" nanowire was then taken out of the SEM for micro-PL measurement. Figure 3(e) compares micro-PL spectra of the unheated nanowire and along different locations of the nanowire after the "burnt-out", showing a dramatically increased green emission and a noticeable UV emission redshift with the temperature increase. The correlation of PL, electrical transport and EDS measurements indicates that the UV emission redshift, green emission, and carrier density are closely related to the oxygen deficiency, which supports native defect complexes and/or hydrogen at oxygen sites serving as stable and effective shallow donor [43, 44].

The deep level emission was also found to be sensitive to the surface condition controlled by growth or sample processing. Figure 4 shows the influence of the surface morphology on the deep level emission in ZnO nanowires with varying diameters. For those nanowires possessing circular cross section and smooth surface [corresponding to straight boundary and uniform contrast in the side view, Fig. 4(a)], the green emission is normally 1–2 orders lower than the UV emission and does not show clear dependence on the nanowires diameters [Fig. 4(b)]. On the other hand, the nanowires with irregular cross section and rough surface (slightly wavy boundary and varying contrast in the side view) usually exhibit much stronger "green" emission intensities accompanied by weakened and redshifted UV emission [Fig. 4(c) and (d)]. Unlike those studies showing anomalous blueshift in UV emission with decreasing nanowire diameter [41, 42], our results show that the UV emission peak energy has little dependence on the diameter but exhibits a strong tendency to redshift with the increase of the "green" defect emission, indicating defect induced modification of the electronic structure or an increased exciton-phonon interaction.

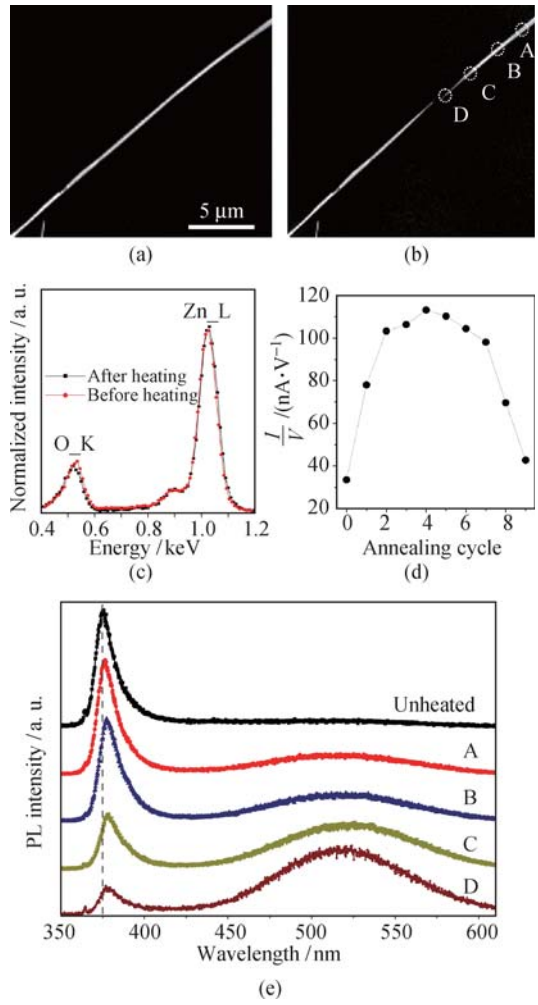

Fig. 3 SEM images showing a suspended ZnO nanowire before **(a)** and after **(b)** *in situ* "burnt-out" by electrical current. **(c)** EDS spectra from position close to the "burnt-out" spot before and after the *in situ* heating. **(d)** Conductance at 7 V as a function of heating cycle. **(e)** Micro-PL spectra from the unheated nanowire and the different positions [marked in Fig. 3(b)] after the "burnt-out". Reprinted with permission from Ref. [18].

For micro-PL studies on individual nanowires, the nanowires are usually sparsely dispersed on a flat substrate [45–47]. The employment of individual suspended nanostructures can effectively avoid the complex influences of the substrates and the often necessary sonication process in solutions. We have observed that the sonication process may cause dramatically decreased UV emission and increased defect emission. Figure 1(c) compares the PL spectra of a sonication processed ZnO nanowire

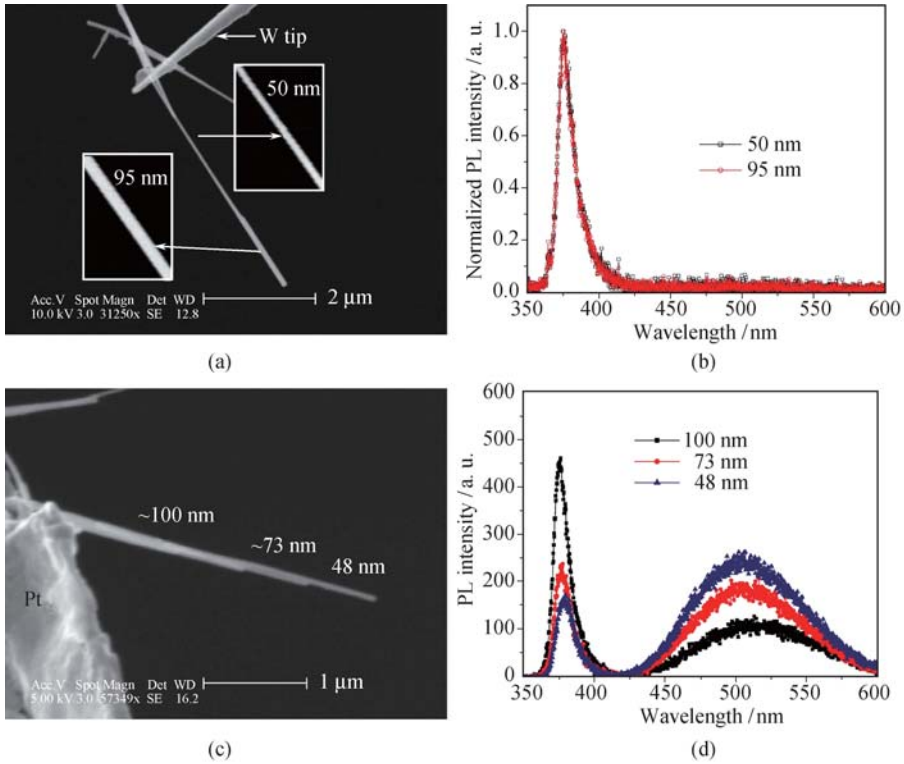

Fig. 4 Side-view SEM images of regular **(a)** and irregular **(c)** shaped individual suspended as-grown ZnO nanowires with changing diameters and the corresponding micro-PL spectra [**(b)** and **(d)**] along their lengths. The insets in (a) show straight boundaries and uniform contrast of the two sections. Reprinted with permission from Ref. [18].

lying on SiO_2/Si substrate and an individual suspended as-grown ZnO nanowire. Much stronger green emission and redshifted NBE emission are observed for the sonication processed ZnO nanowire, likely being resulted from the surface change of the nanowire after solution sonication.

4 Characterization of optical confinement in 1-D ZnO nanostructures

1-D nanostructures may exhibit confinement on the photons or excitons, especially in the radial direction, which results in intriguing anisotropic optical properties. The optical confinement plays important roles in the reported optoelectronic nanodevices based on 1-D nanostructures, for example, light emitting diodes [48], nanolasers [6, 9, 16, 17] and waveguides [8, 49]. Photoluminescence (PL) imaging, and spatially resolved PL spectroscopy using confocal and scanning near field optical microscopes have been employed to study the emission from the ends and the sidewall positions of 1-D nanostructures [29, 50–55]. For such measurements on individual 1-D nanostructures, the direction of the luminescence collection was fixed to be perpendicular to the axis of the 1-D nanostructures. Such experimental condition limits the excitation and detection angles relative to the individual nanorods/nanowires so that the direction perpendicular to the nanorod/nanowire axis is usually the only practical direction for both excitation and detection. Here we show that by using the techniques described in this paper, the angular dependent PL measurement of an individual nanostructure can be achieved.

First, we employ micro-PL spectroscopy on the "nanostructure-on-a-tip" samples prepared by *in situ* nanoprobe technique. The flexibility of the individual suspended nanostructures attached to sharp metal tips allows large angle rotation and tilting, which makes it possible to carry out angular dependent micro-PL measurements on individual nanorods. In Fig. 5 we show micro-PL spectra acquired along the perpendicular and parallel to the axis of the same individual suspended nanorod. The emission from the parallel direction can be two orders of magnitude higher than that from the perpendicular direction, which demonstrates the waveguiding efficiency quantitatively [56].

For a standard micro-PL setup, an objective lens is used for both excitation and signal collection, thus the excitation and collection directions cannot be separated for a large angle. In contrast, the integrated system (Fig. 2) hires separated excitation (the electron beam) and collection (the fiber probe). In addition, the fiber probe has an adjustable collection angle. Thus, more flexible and quantitative characterization on the anisotropic light emitting properties of nanostructures can be achieved. In Fig. 6, we show angular resolved CL spectra of a single ZnO nanorod at different orientations with respect to the fiber probe. By rotating the sample stage, the angle

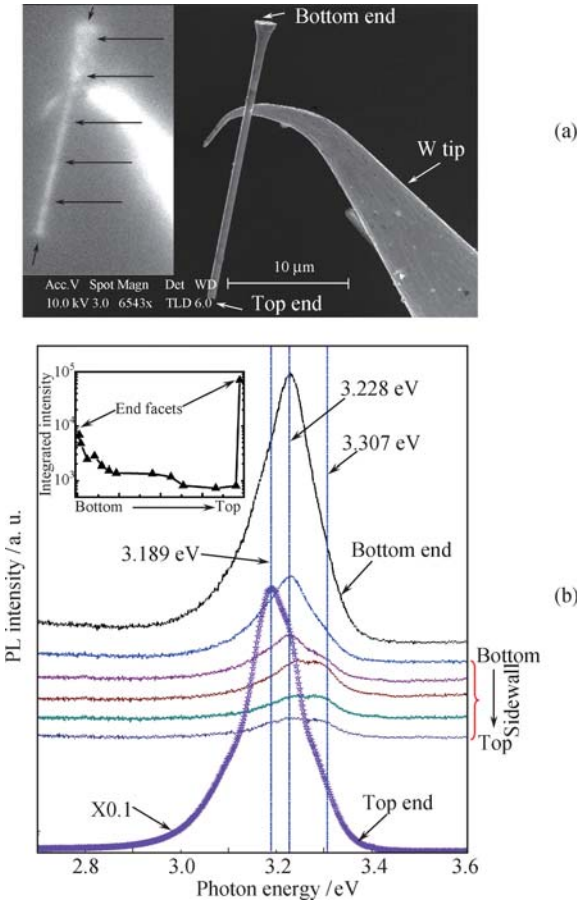

Fig. 5 **(a)** SEM and optical (the inset) images of the same individual suspended ZnO nanorod of 659 nm in diameter. **(b)** Micro-PL spectra from both sidewall positions and end facets indicated by the arrows in the optical image in (a). The inset shows the variations of integrated intensity of the NBE emissions from end facets and sidewall positions of the nanorod. Reprinted with permission from Ref. [56].

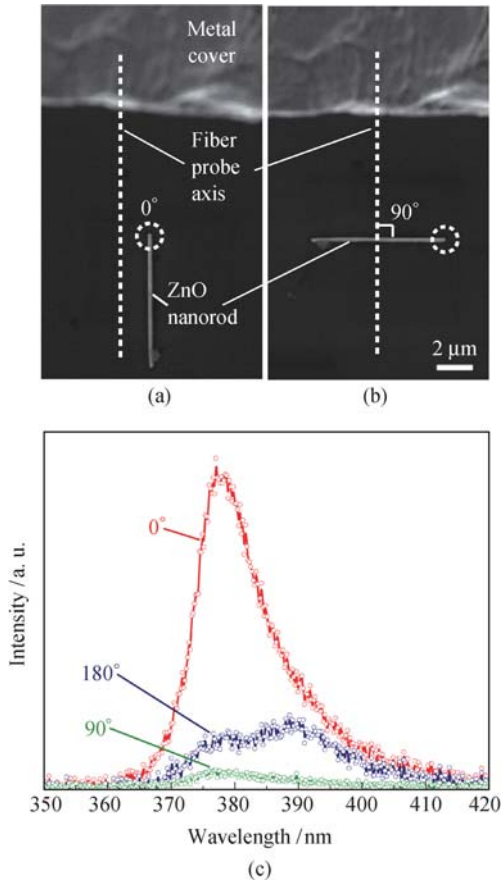

Fig. 6 Angular resolved CL measurements of a single ZnO nanorod. **(a)** and **(b)** SEM images showing the same ZnO nanorod at 0° and 90° angles with respect to the projection of the fiber probe axis. **(c)** CL spectra of the same position near one end of the ZnO nanorod [marked by *dashed circle* in (a) and (b)] obtained at 0°, 90° and 180° orientation angles respectively. Reprinted with permission from Ref. [17].

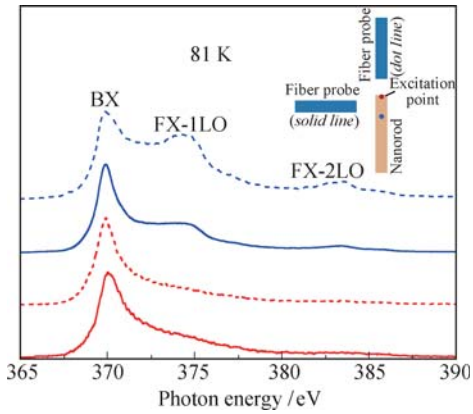

Fig. 7 Spatially and angularly resolved CL spectra (*normalized*) of a single ZnO nanorod at 81 K. The colors of the spectra correspond to different excitation points and the line shapes (*solid* and *dotted*) denote the detection orientations as illustrated in the inset.

between the nanorod axis and the projection of the fiber axis on the substrate can be varied [Fig. 6(a) and (b)]. Figure 6(c) shows CL spectra taken with the electron beam focused on the same position near one end of the nanorod for the orientation angles of 0° [Fig. 6(a)], 90° [Fig. 6(b)], and 180°, respectively. It is found that the CL intensity reaches a minimum at 90° (∼17 times lower than that at 0°), while a redshifted NBE emission peak is observed at 180°. These results are in good agreement with the waveguiding behavior of the ZnO nanorods [8, 56]. The generated light mainly propagates along the nanorod axis (*c* axis) and exits from the two end facets of the nanorod. To further understand the redshift caused by longer propagation distance, similar measurements have been carried out at 81 K, and the results are shown in Fig. 7. As the propagation distance increases, the LO phonon replicas of the free excitons (FX-1LO) are enhanced dramatically, indicating that the redshift of the NBE emission at room temperature is caused by the increased spectral weight of the LO phonon replicas.

The above results are consistent with our micro-PL measurements on the nanorod Fabry–Pérot cavities, which demonstrate the important role of LO phonons in the exciton polariton relaxation [55]. In addition, the waveguiding behavior and the redshift due to the enhanced exciton-phonon interaction can also be used to explain some observed anomalous blueshift of the NBE emission at reduced nanowires/nanorod diameters. For example, Fig. 8 shows macro-PL spectra from arrays

of ZnO nanorods with average diameters ranging from 450 nm to 80 nm [57]. The room temperature NBE emissions show gradual blueshift with the decreasing diameter. However, the temperature dependent PL show that the peak positions of the FX and FX-nLO emissions are the same for different samples at 10 K, while the blueshift of the smaller diameter samples are caused by the reduced exciton-phonon interaction due to the degraded waveguiding properties for small diameter nanorods [58].

5 *In situ* assembly and characterization of optoelectronic nanostructures for device purposes

The above integrated system also allows *in situ* assembly and characterization of nanostructures with simple optoelectronic functions. Figure 9 shows the assembly and characterization of an *in situ* light emitter based on a single n-ZnO nanowire dispersed on p^+-Si substrate. Figure 9(a) and (b) are the top-view SEM image and the side-view schematic of the assembled structure, respectively. A W tip is driven by a nano-manipulator to make contact with the nanorod. An electrical voltage is applied between the W tip and the substrate. I–V measurement indicated a typical p–n junction characteristic [19]. Because of the unfavorable band alignment [59], no luminescence has been detected in the contact mode even at an injection current of tens of μA. However, as the W tip was moved upward to form a nanometer-sized gap between the nanorod and the tip, strong tunneling-induced luminescence was observed at a >30 V positive voltage between the substrate and the W tip. The corresponding tunneling current was about several μA. The tunneling luminescence shows dominating narrow NBE emission, indicating a potential application in high efficiency narrowband UV light emitting nanodevices [Fig. 9(d)].

In Fig. 10, we demonstrate the assembly and characterization of an *in situ* photodetector based on an individual suspended Bi_2S_3 nanowire placed between two W tips [Fig. 10(a)] via *in situ* nano-manipulation [19, 60]. A laser beam (633-nm He–Ne laser) was used to illuminate the nanowire through a fiber probe. A constant 5-V voltage was applied to the nanowire. Figure 10(b) shows that varied excitation intensity leads to a current variation between 23 nA and 113 nA due to the generated extra carriers.

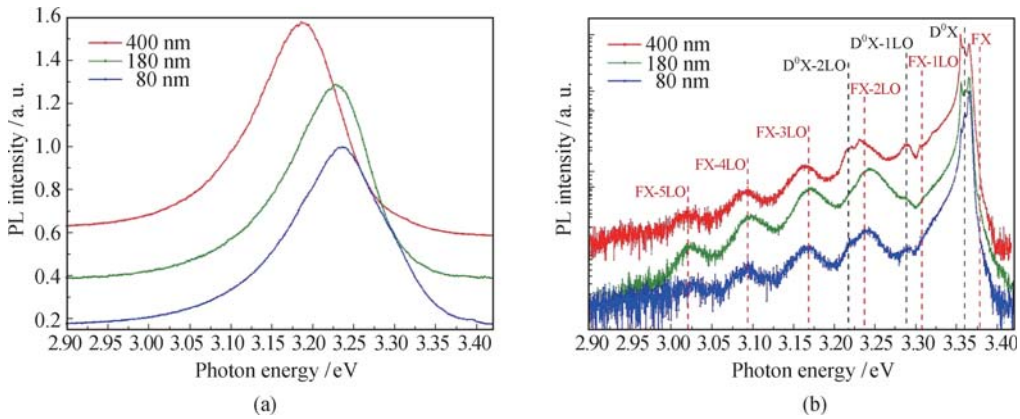

Fig. 8 Intensity normalized PL emission spectra of ZnO nanorod arrays with different average diameters at room temperature **(a)** and at 10 K **(b)**. Reprinted with permission from Ref. [17].

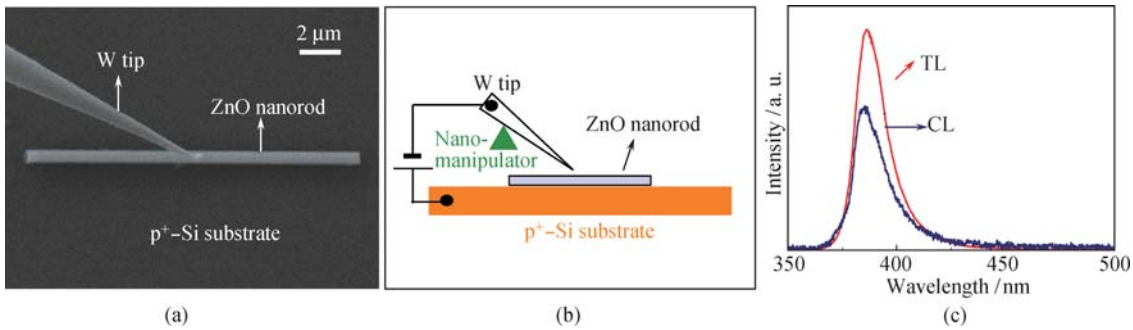

Fig. 9 Characterization of an *in situ* light emitter based on a single ZnO nanorod. **(a)** Top-view SEM image of an individual ZnO nanorod dispersed on p^+–Si substrate. The W tip is controlled by a nano-manipulator and placed above the nanorod. **(b)** Side-view schematic diagram of the light emitter. **(c)** Tunneling luminescence (TL) spectrum obtained at the presence of a nanometer-sized gap between the ZnO nanorod and the W tip. A CL spectrum from the same nanorod is also presented for comparison. The two luminescence spectra are normalized according to the excitation power, showing that the tunneling luminescence has a high efficiency comparable to the CL excited by 10 keV electrons. Reprinted with permission from Ref. [19].

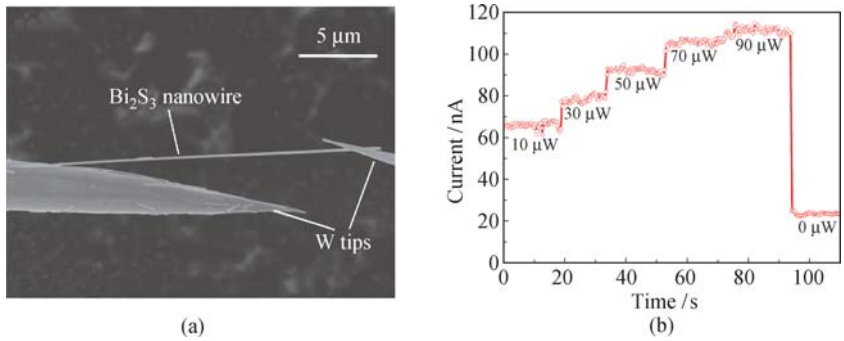

Fig. 10 Assembly and Characterization of an *in situ* photodetector based on a single Bi_2S_3 nanowire. **(a)** SEM image of an individual Bi_2S_3 nanowire suspended between two sharp W tip electrodes. **(b)** Typical electrical response of the individual suspended Bi_2S_3 nanowires to 633-nm laser illumination. A constant 5-V voltage is applied to the nanowire. Reprinted with permission from Ref. [19].

Such *in situ* technique with high flexibility and efficiency can be developed into an effective route to explore optoelectronic nanodevices, especially in building prototype devices and selecting suitable nanostructures for device purposes. Compared to the typical nanodevice fabrication process, the above *in situ* assembly and characterization technique can avoid some complications, e.g., nanostructure dispersion, lithography, vacuum plating, and lift-off due to its simple process.

6 Summary

In this paper, we review our recent progress of *in situ* characterization of optoelectronic nanostructure and nanodevices. By combining optical techniques and *in situ* scanning electron microscopy, we have developed two approaches allowing comprehensive microstructural, compositional, electrical and optical characterization of the same 1-D nanostructure. The first approach is to locate and characterize the same individual nanostructure in a compatible sample using a variety of characterization techniques. The second is to assemble an integrated system by combining optical fiber probe and *in situ* SEM techniques. By using these two techniques, the origin of the deep level emission in ZnO nanowires and the waveguiding behavior of the ZnO nanorods were studied. In addition, the integration approach allows *in situ* assembly and characterization of optoelectronic nanostructures for device purposes. Using the above examples, we demonstrate that the combination of optical techniques and *in situ* electron microscopy can be a powerful tool for nanomaterial and nanodevice studies.

Acknowledgements This work was supported in part by the State Key Development Program for Basic Research of the Ministry of Science and Technology of China (Grant Nos. 2006CB932401 and 2006AA03Z350), the National Natural Science Foundation of China (Grant No. 50702002), and SRF for ROCS, SEM.

References

1. X. Duan, Y. Huang, Y. Cui, J. Wang, and C. M. Lieber, Nature, 2001, 409: 66
2. R. Agarwal and C. M. Lieber, Appl. Phys. A, 2006, 85: 209
3. Y. Li, F. Qian, J. Xiang, and C. M. Lieber, Materials Today, 2006, 9: 18
4. R. X. Yan, D. Gargas, and P. D. Yang, Nature Photonics, 2009, 3: 569
5. M. A. Zimmler, D. Stichtenoth, C. Ronning, W. Yi, V. Narayanamurti, T. Voss, and F. Capasso, Nano Lett., 2008, 8: 1695
6. M. H. Huang, S. Mao, H. Feick, H. Yan, Y. Wu, H. Kind, E. Weber, R. Russo, and P. D. Yang, Science, 2001, 292: 1897
7. H. Kind, H. Yan, B. Messer, M. Law, and P. D. Yang, Adv. Mater., 2002, 14: 158
8. M. Law, D. J. Sirbuly, J. C. Johnson, J. Goldberger, R. J. Saykally, and P. D. Yang, Science, 2004, 305: 1269
9. X. Duan, Y. Huang, R. Agarwal, and C. M. Lieber, Nature, 2003, 421: 241
10. H. Zhou, M. Wissinger, J. Fallert, R. Hauschild, F. Stelzl, C. Klingshirn, and H. Kalt, Appl. Phys. Lett., 2007, 91: 181112
11. R. F. Oulton, V. J. Sorger, T. Zentgralf, R. M. Ma, C. Gladden, L. Dai, G. Bartal, and X. Zhang, Nature, 2009, 461: 629
12. C. Soci, A. Zhang, B. Xiang, S. A. Dayeh, D. P. R. Aplin, J. Park, X. Y. Bao, Y. H. Lo, and D. Wang, Nano Lett., 2007, 7: 1003
13. B. Tian, X. Zheng, T. J. Kempa, Y. Fang, N. Yu, G. Yu, J. Huang, and C. M. Lieber, Nature, 2007, 449: 885
14. M. R. Lee, R. D. Eckert, K. Forberich, G. Dennler, C. J. Brabec, and R. A. Gaudiana, Science, 2009, 324: 232
15. L. Tong, R. R. Gattass, J. B. Ashcom, S. He, J. Lou, M. Shen, I. Maxwell, and E. Mazur, Nature, 2003, 426: 816
16. A. L. Pan, W. C. Zhou, E. S. P. Leong, R. B. Liu, A. H. Chin, B. S. Zou, and C. Z. Ning, Nano Lett., 2009, 9: 784
17. J. Dai, C. X. Xu, K. Zheng, C. G. Lv, and Y. P. Cui, Appl. Phys. Lett., 2009, 95: 241110
18. M. Gao, W. L. Li, Y. Liu, Q. Li, Q. Chen, and L. M. Peng,

Appl. Phys. Lett., 2008, 92: 113112
19. C. Y. Li, M. Gao, C. Ding, X. X. Zhang, L. H. Zhang, Q. Chen, and L. M. Peng, Nanotechnology, 2009, 20: 175703
20. S. Frank, P. Poncharal, Z. L. Wang, and W. A. de Heer, Science, 1998, 280:1744
21. M. S. Wang, J. Y. Wang, Q. Chen, and L. M. Peng, Adv. Funct. Mater., 2005, 15:1825
22. L. M. Peng, Q. Chen, X. L. Liang, S. Gao, J. Y. Wang, S. Kleindiek, and S. W. Tai, MICRON, 2004, 35: 495
23. Y. Liu, S. Wang, Z. Y. Zhang, L. M. Peng, L. Shi, and Q. Li, Appl. Phys. Lett., 2008, 92: 033102
24. Q. Chen, S. Wang, and L. M. Peng, Nanotechnology, 2006, 17: 1087
25. X. L. Wei, Y. Liu, Q. Chen, and L. M. Peng, Nanotechnology, 2008, 19: 355304
26. H. Kalt, Lect. Notes Phys., 2005, 658: 51
27. J. C. Kim, H. Rho, L. M. Smith, H. E. Jackson, S. Lee, M. Dobrowolska, and J. K. Furdyna, Appl. Phys. Lett., 1999, 75: 214
28. A. Gustafsson, M. E. Pistol, L. Montelius, and L. J. Samuelson, Appl. Phys., 1998, 84: 1715
29. D. Liu, A. L. Pan, G. Z. Xu, Y. Q. Bai, X. Zhu, and B. S. Zou, Opt. Rev., 2006, 13: 235
30. S. A. Empedocles, R. Neuhauser, K. Shimizu, and M. G. Bawendi, Adv. Mater., 1999, 11: 1243
31. J. B. Baxter, F. Wu, and E. S. Aydil, Appl. Phys. Lett., 2003, 83: 3797
32. X. B. Han, L. Z. Kou, X. L. Lang, J. B. Xia, N. Wang, R. Qin, J. Lu, J. Xu, Z. M. Liao, X. Z. Zhang, X. D. Shan, X. F. Song, J. Y. Gao, W. L. Guo, and D. P. Yu, Adv. Mater., 2009, 21: 4937
33. P. M. Petroff and D. W. Lang, Appl. Phys. Lett., 1977, 31: 60
34. B. G. Yacobi and D. B. Holt, Cathodoluminescence Microscopy of Inorganic Solids, New York: Springer-Verlag, 1990: 116
35. Y. Ohno and S. Takeda, Rev. Sci. Instrum., 1995, 66: 4866
36. L. J. Brillson, J. Vac. Sci. Technol. B, 2001, 19: 1762
37. M. Gao, S. T. Bradley, Y. Cao, D. Jena D, Y. Lin Y, S. A. Ringel, J. Hwang, W. J. Schaff, and L. J. Brillson, J. Appl. Phys., 2006, 100: 103512
38. A. B. Djurišić and Y. H. Leung, Small, 2006, 2: 944
39. K. Vanheusden, W. L. Warren, C. H. Seager, D. R. Tallant, J. A. Voigt, and B. E. Gnade, J. Appl. Phys., 1996, 79: 7983
40. A. B. Djurišić Y. H. Leung, K. H. Tam, Y. F. Hsu, L. Ding, W. K. Ge, Y. C. Zhong, K. S. Wong, W. K. Chan, H. L. Tam, K. W. Cheah, W. M. Kwok, and D. L. Phillips, Nanotechnology, 2007, 18: 095702
41. C. W. Chen, K. H. Chen, C. H. Shen, A. Ganguly, L. C. Chen, J. J. Wu, H. I. Wen, and W. F. Pong, Appl. Phys. Lett., 2006, 88: 241905
42. P. C. Chang, C. J. Cheien, D. Stichtenoth, C. Ronning, and J. G. Lu, Appl. Phys. Lett., 2007, 90: 113101
43. D. C. Look, G. C. Farlow, S. Limpijumnong, S. B. Zhang, and K. Nordlund, Phys. Rev. Lett., 2005, 95: 225502
44. A. Janotti and C. G. Van de Walle, Appl. Phys. Lett., 2005, 87: 122102
45. M. Freitag, J. Chen, J. Tersoff, J. C. Tsang, Q. Fu, J. Liu, and P. Avouris, Phys. Rev. Lett., 2004, 93: 076803
46. J. F. Wang, M. S. Gudiksen, X. F. Duan, Y. Cui, and C. M. Lieber, Science, 2001, 293: 1455
47. L. Wischmeier, T. Voss, S. Börner, and W. Schade, Appl. Phys. A, 2006, 84: 111
48. F. Qian, S. Gradecak, Y. Li, C. Y. Wen, and C. M. Liber, Nano Lett., 2005, 5: 2287
49. C. J. Barrelet, A. B. Greytak, and C. M. Lieber, Nano Lett., 2004, 4: 1981
50. L. K. van Vugt, S. Rühle, P. Ravindran, H. C. Gerritsen, L. Kuipers, and D. Vanmaekelbergh, Phys. Rev. Lett., 2006, 97: 147401
51. S. Rühle, L. K. van Vugt, H. Y. Li, N. A. Keizer, L. Kuipers, and D. Vanmaekelbergh, Nano Lett., 2008, 8: 119
52. J. C. Johnson, H. Yan, P. Yang, and R. J. Saykally, J. Phys. Chem. B, 2003, 107: 8816
53. T. Voss, G. T. Svacha, E. Mazur, S. Müller, C. Ronning, D. Konjhodzic, and F. Marlow, Nano Lett., 2007, 7: 3675
54. R. M. Ma, X. L. Wei, L. Dai, S. F. Liu, T. Chen, S. Yue, Z. Li, Q. Chen, and G. G. Qin, Nano Lett., 2009, 9: 2697
55. W. L. Li, M. Gao, X. X. Zhang, D. F. Liu, L. M. Peng, and S. S. Xie, Appl. Phys. Lett., 2009, 95: 173109
56. W. L. Li, M. Gao, R. Cheng, X. X. Zhang, S. S. Xie, and L. M. Peng, Appl. Phys. Lett., 2008, 93: 023117
57. X. X. Zhang, D. F. Liu, L. H. Zhang, W. L. Li, M. Gao, W. J. Ma, Y. Ren, Q. S. Zeng, Z. Q. Niu, W. Y. Zhou, and S. S. Xie, J. Mater. Chem., 2009, 19: 962
58. J. C. Johnson, H. Q. Yan, P. D. Yang, and R. J. Saykally, J. Phys. Chem. B, 2003, 107: 8816
59. J. Bao, M. A. Zimmler, and F. Capasso, Nano Lett., 2006, 6: 1719
60. Y. Yu, C. H. Jin, R. H. Wang, Q. Chen, and L. M. Peng, J. Phys. Chem. B, 2005, 109: 18772